

WIGNER LATTICE ORDER, COLLECTIVE MODE, AND SUPERCONDUCTIVITY IN $\text{La}_{1.985}\text{Sr}_{0.015}\text{CuO}_{4+\delta}$ SYSTEM

YOUNG HOON KIM¹ and PEI HERNG HOR²

¹ Department of Physics, University of Cincinnati, Cincinnati, Ohio 45221-0011, U.S.A.

² Department of Physics and Texas Center for Superconductivity, University of Houston Houston, Texas 77204-5002, U.S.A.

Published on Modern Physics Letters B, Vol. 15, No. 15 (2001) 497-513

We have studied far-infrared charge dynamics of Sr- and O- co-doped $\text{La}_{1.985}\text{Sr}_{0.015}\text{CuO}_{4+\delta}$ with $\delta = 0.024$ ($p = 0.063$ per Cu) and $\delta = 0.032$ ($p = 0.07$). We found that two-dimensional Wigner lattice order is the ground state of cuprates away from half-filling. We found that the presence of 2D Wigner lattice and the pinned Goldstone mode is essential for the cuprate physics and superconductivity. We propose that all the high T_c physics are based on the existence of these peculiar 2D electron lattices.

Superconductivity in layered copper-oxides (cuprates) has been one of the important problems in condensed matter physics that still awaits the answer for the underlying mechanism(s) that drives this doped insulator to a superconductor with high transition temperature (T_c). Theoretically, the main problem has been finding an adiabatic connection between the antiferromagnetic order and superconducting order in the quasi two-dimensional (2D) CuO_2 planes upon hole doping. On the antiferromagnetic insulating side, the t-J model,¹ which is derived from the Hubbard model,² has been believed to capture the essential physics of CuO_2 planes. As the system is doped with holes, Anderson proposed³ that the Mott-Hubbard insulator becomes a 2D Luttinger liquid where the spin and charge of electrons are separated into spinons and holons. Later, a philosophically different $\text{SO}(5)$ theory was proposed by Zhang,⁴ which is a microscopic model with a five-component order parameter that embraces both the antiferromagnetic order corresponding to a charge zero, spin 1 particle-hole pair at half-filling ($p = 0$) and the superconducting order corresponding to a charge $\pm 2e$ cooper pair spin singlet away from half-filling. Experimentally, besides antiferromagnetism and superconductivity, spin clusters, spin glass and a highly elusive hole concentration (p)-independent pseudogap in spin

excitation and charge spectra are observed in the normal state.⁵ Based on the observed rich physical phenomena, a generic electronic phase diagram has been generated as a function of temperature and hole concentration.⁶ Although it is widely recognized that studying this phase diagram holds the key to understand the cuprate physics, until now no theory has been able to account for the mere existence of such a phase diagram.

In a recent cation and anion co-doping study of the general properties of the electronic phase diagram, incipient electronic instabilities related to energetically favored electronic phases were identified at special hole concentrations (p_s).⁷ In particular, a $p_s = 1/16$ is observed. This $p_s = 1/16$ corresponds to a previously reported critical hole concentration (p_c) which dictates the doping efficiency and signals a chemical potential jump of the doped holes.⁸ This $p_c = 1/16$ is also the point where superconductivity first appears in the phase diagram. In Fig.1 we present the onset T_c vs. p curves of $\text{La}_{2-x}\text{Sr}_x\text{CuO}_{4+\delta}$ for $x = 0, 0.015$, and 0.05 . The T_c is defined as the onset temperature of the Meissner effect. The p of each sample series is varied precisely by small steps of $\Delta p = 0.0025 \sim 0.004$ using electrochemical oxidation to change the oxygen concentration, δ .⁸ While a single 30K transition is observed for x

$= 0$ samples, a dramatic increase of T_c from $\sim 15\text{K}$ to $\sim 30\text{K}$ is clearly seen for both $x = 0.015$ and 0.05 samples. In particular, for the $x = 0.015$ sample it is remarkable to observe an almost discontinuous jump from $T_c \sim 16\text{K}$ to 26K by a very small change of carrier concentration $\Delta p = 0.004$ near p_c . Since $p_c = 1/16$ is a special carrier concentration related to a possible electronic phase instability, far-infrared studies of the $x = 0.015$ sample at various p across p_c provides a unique opportunity to investigate the specific role of this instability to the normal state charge dynamics and to the occurrence of the superconductivity in cuprates.

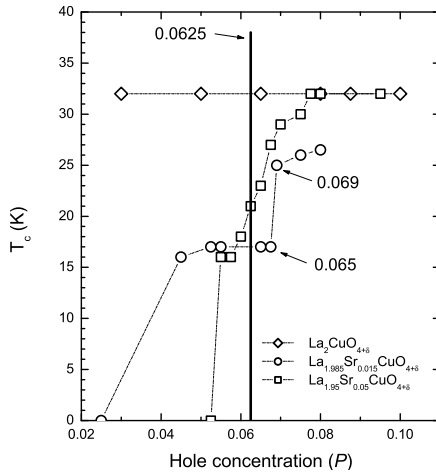


Figure 1. Superconducting onset temperature (T_c) versus hole concentration (p)

The nature of charge carriers in the CuO_2 planes (ab-planes) and their interactions may be directly probed by far-infrared reflectivity measurements. However, because of the Drude-like free-carrier contributions to the far-infrared conductivity, the normal state reflectivity is rather featureless. The only persistent characteristic spectral feature found was the emergence of a doping-independent "knee"-like structure in the

reflectivity at $\sim 400\text{ cm}^{-1}$ ($\sim 50\text{ meV}$) upon cooling the sample below T_c .⁹ This structure manifests itself as a broad dip in the frequency dependent conductivity for $T < T_c$. The physical origin of the dip has not been resolved.^{10,11} Recently, the dip in $\text{YBa}_2\text{Cu}_3\text{O}_{7-\delta}$ systems has been attributed to the coupling of electrons to the 41 meV resonance peak observed in neutron scattering.¹² Also, it was found that there exists substantial residual conductivity in the far-infrared below the dip frequency (ω) $\sim 400\text{ cm}^{-1}$ even for $T < T_c$. The physical nature of this residual background conductivity and its relevance to the superconductivity has not been understood.

Studies of photoinduced carriers in undoped cuprate provide an alternative approach to understand the nature of charge carriers and their interactions with the lattice. Because there is no Drude conductivity, one can clearly discern the carrier-induced background conductivities. Although the spectral features for $\omega < 200\text{ cm}^{-1}$ could not be resolved due to the nature of the experiments, the infrared photoinduced absorption measurements of La_2CuO_4 and Nd_2CuO_4 revealed that the photocarriers became self-localized via coupling to the lattice as evidenced by the photoinduced infrared-active vibrational modes.¹³ Also, there existed an accompanying electronic excitation peak at $\sim 1000\text{ cm}^{-1}$ ($\sim 0.12\text{ eV}$) with an onset at $\sim 400\text{ cm}^{-1}$. This result was interpreted as the result of phase separation of the photocarriers in the CuO_2 planes into hole-rich domains with local p comparable to that of optimally doped cuprates.¹⁴

In this work, we investigated two polycrystalline $x = 0.015$ samples at either side of the T_c jump near p_c . In preparing the sample, different electrochemical oxidation techniques have been carefully evaluated¹⁵ and the thermodynamic equilibrium properties of the electrochemical intercalation of oxygen into polycrystalline $\text{La}_{2-x}\text{Sr}_x\text{CuO}_{4+\delta}$ system have been studied.¹⁶ Because of the strong anisotropic nature of cuprates where the electromagnetic response is nearly insulating for polarization parallel to the c-axis and conducting for polarization parallel to the ab-plane and because the c-axis far-infrared

properties of single crystalline $\text{La}_{2-x}\text{Sr}_x\text{CuO}_4$ are well-documented,¹⁷ we were able to unambiguously identify the in-plane far-infrared charge dynamics of polycrystalline $\text{La}_{1.985}\text{Sr}_{0.015}\text{CuO}_{4+\delta}$ sample, which is directly relevant to the normal and superconducting states.

We have carried out far-infrared reflectivity measurements of two different samples of $\text{La}_{1.985}\text{Sr}_{0.015}\text{CuO}_{4+\delta}$ near p_c as a function of temperature for ω between $\sim 7 \text{ cm}^{-1}$ and 5000 cm^{-1} ; one with $\delta = 0.024$ (or $p = 0.063$ per Cu) which undergoes the superconducting transition at $T_c = 16 \text{ K}$ and the other at $\delta = 0.032$ (or $p = 0.07$ per Cu) with $T_c = 26 \text{ K}$ defined as the onset temperature of the Meissner effects shown in the inset of Figure 2a and 2b, respectively. Both resistivity ρ vs. T and $d\rho/dT$ vs. T curves are depicted in Figures 2a and 2b. Although they have quite different T_c 's, one interesting feature in both $d\rho/dT$ vs. T curves is a common minimum and maximum observed at $\sim 200 \text{ K}$ and $\sim 150 \text{ K}$. These very similar behaviors suggest that the same physics is in operation for the normal state in both samples. We noted that the Meissner effect signal size of $\delta = 0.032$ sample is larger than that of $\delta = 0.024$ sample. This result indicates that the superconducting state in the $\delta = 0.032$ sample is not due to the formation of oxygen-rich phase. A smaller Meissner effect is expected since there will be a smaller superconducting volume for samples chemically phase-separated into oxygen rich domains. Indeed, there are only two T_c 's, one at $\sim 15 \text{ K}$ and the other at $\sim 30 \text{ K}$, observed for the entire underdoped regime in the pure oxygen doped equilibrium samples.¹⁸ This indicates, besides two chemical phases, that two T_c 's might be coming from two different electronic phases.

In this experiment, we directly measured the sample temperature from the backside of the sample. The temperature resolution was $(1 \pm 0.1) \text{ K}$ for $T < 40 \text{ K}$. Far-infrared properties, represented by a complex dielectric function

$$\epsilon(\omega) = \epsilon_1(\omega) + 4\pi i\sigma_1(\omega)/\omega \quad (1)$$

have been calculated from a Kramers-Kronig analysis of the measured reflectivities. For $\omega < 7 \text{ cm}^{-1}$, we used an empirical extrapolation scheme

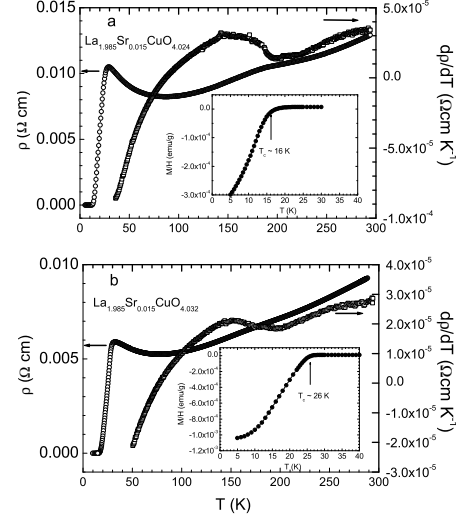


Figure 2. Resistivity and first derivative of resistivity versus temperature curves for oxygen codoped polycrystalline

$R(\omega) \approx 1 - C\omega^{\frac{1}{2}+\delta}$ with $-1/2 \leq \delta \leq 1/2$ subject to $\sigma_1(\omega \rightarrow 0) = \sigma_{dc}$ where σ_{dc} is the measured dc conductivity.¹⁹

Far-infrared reflectivities of $\delta = 0.024$ and $\delta = 0.032$ samples are shown in Figure 3 at selected temperatures. Besides the contribution due to the well-known in-plane mode at $\sim 500 \text{ cm}^{-1}$ and the intense c-axis phonon mode at $\omega \sim 220 \text{ cm}^{-1}$ and a weak mode at $\sim 350 \text{ cm}^{-1}$, there appears a sharp minimum in the reflectivity at $\omega \sim 16 \text{ cm}^{-1}$ that resembles the reflectivity curve in the vicinity of the plasma edge of a free electron gas and several unusual notable features. Below the minimum at $\omega \sim 16 \text{ cm}^{-1}$ the reflectivity approaches unity as ω approaches zero. For $\delta = 0.024$ sample, a bump at $\omega \sim 25 \text{ cm}^{-1}$ is evident and another weak broad feature located at $\omega \sim 100 \text{ cm}^{-1}$ on which a sharp peak develops as T decreases. We noted that the reflectivity does not approach unity for frequencies down to $\omega \sim 7 \text{ cm}^{-1}$ even in the superconducting state.

For $\delta = 0.032$ sample, in addition to what have already been seen for $\delta = 0.024$ sample, two ad-

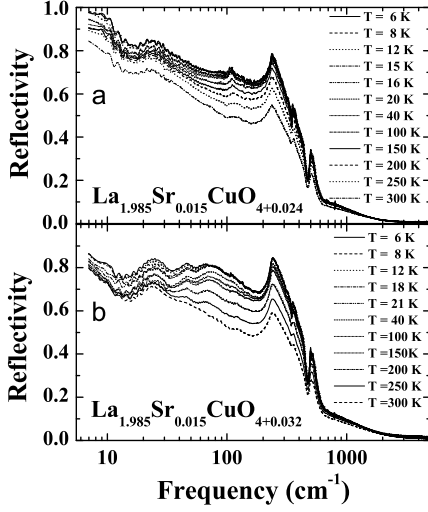


Figure 3. Reflectivity versus frequency curves at various temperatures: (a) $\delta = 0.024$ sample and (b) $\delta = 0.032$ sample.

ditional bumps are present: one at $\omega \sim 45 \text{ cm}^{-1}$ and the other at $\omega \sim 80 \text{ cm}^{-1}$. One remark on the reflectivity data is that because we use polycrystalline sample, there exist possible errors in determining the absolute reflectivity at $\omega \rightarrow 0$ due to the overestimation of the reflectivity. We were unable to determine the reflectivity of $\delta = 0.032$ sample for $\omega < 10 \text{ cm}^{-1}$ to the desired accuracy ($< 1\%$). During the course of this experiment, we found that the reflectivity in the spectral range between 100 cm^{-1} and 600 cm^{-1} are close to true reflectivity of the sample. The uncertainty of the far-infrared reflectivity of $\delta = 0.032$ sample for $\omega < 10 \text{ cm}^{-1}$ is slightly higher than that of $\delta = 0.024$ sample ($\sim 1\%$). However, this error does not affect our conclusions for $\omega > 10 \text{ cm}^{-1}$.

The Kramers-Kronig derived real part of conductivity $\sigma_1(\omega)$ and the real part of dielectric function $\epsilon_1(\omega)$ of $\delta = 0.024$ sample are displayed in Figure 4a & 4b at various T, respectively. In $\sigma_1(\omega)$, there appear a sharp upturn approaching σ_{dc} in $\sigma_1(\omega)$ below 10 cm^{-1} and an extremely sharp (FWHM $\sim 10 \text{ cm}^{-1}$) peak located at ω

$\sim 23 \text{ cm}^{-1}$ whose strength increases as T decreases. We can also observe a broad mode at $\sim 90 \text{ cm}^{-1}$ that becomes pronounced at low T and an electronic excitation peak at $\sim 1000 \text{ cm}^{-1}$ with an onset at $\sim 400 \text{ cm}^{-1}$. All these features exist in addition to the well-known ab-plane and c-axis CuO_2 phonon modes. We identify this electronic excitation peak with the lower energy electronic excitation in the photoinduced infrared absorption measurements. All these features in $\sigma_1(\omega)$ develop on top of a constant, rather frequency independent background conductivity of $\sim 10 \Omega^{-1}\text{cm}^{-1}$ which presumably comes from the c-axis contribution.

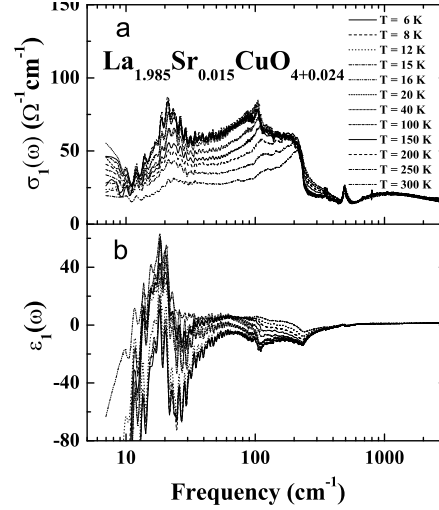


Figure 4. Kramers-Kronig derived (a) real part of the conductivity $\sigma_1(\omega)$ and (b) real part of the dielectric function $\epsilon_1(\omega)$ for $\delta = 0.024$ sample.

From the $\epsilon_1(\omega)$ plot in Figure 4b, it is clear that the reflectivity minimum at $\sim 16 \text{ cm}^{-1}$ arises from the zero crossing of the $\epsilon_1(\omega)$ and there is no sign of any corresponding structure seen in the conductivity. Therefore, we assign the reflectivity minimum as the plasma edge due to the free carriers with screened plasma frequency $\omega_p \sim 16$

cm^{-1} . By assuming the free carrier mass to be the electron mass and using the static dielectric constant $\epsilon_1(0) \sim 40$ estimated from $\epsilon_1(\omega)$ at 300 K, we find the free carrier concentration $n_F \sim 2.3 \times 10^{17} \text{ carriers/cm}^3$ which is only $\sim 0.4\%$ of the total carriers in the system. Even though the measured σ_{dc} is in the range of $\sim 100 \Omega^{-1}\text{cm}^{-1}$ and the observed $\sigma_1(\omega)$ is the average between the ab-plane and c-axis conductivities, the sharp upturn in $\sigma_1(\omega)$ toward σ_{dc} at $\omega < 10 \text{ cm}^{-1}$ indicates that the free carriers experience virtually no scattering ($\Gamma \sim 4 \text{ cm}^{-1}$). This observation suggests that the extremely small fraction of free carriers participate in a coherent charge transport in $\text{La}_{1.985}\text{Sr}_{0.015}\text{CuO}_{4+\delta}$.

The $\epsilon_1(\omega)$ of $\delta = 0.024$ sample clearly reveals that the $\omega \sim 23 \text{ cm}^{-1}$ mode is a collective mode (ω_{GL}) and the 400 cm^{-1} is the corresponding single particle excitation gap (2Δ). One might consider that the origin of this collective mode is from a spin density wave (SDW). However, in this event the entire spectral weight is expected to move to the collective mode of the SDW because the dynamic mass of the SDW is the free electron mass. That is, we do not expect to have the single particle excitation peak. Therefore, this collective mode is resulting from the charge condensation into a one-dimensional or 2D density wave in the CuO_2 planes and this density wave is pinned as evidenced by the finite frequency of the collective mode.

The spectral weight distribution indicates that almost all the carriers introduced to the CuO_2 planes are spent to form a pinned charge density wave (CDW). Since a pinned CDW is an insulator,²⁰ the pinned CDW itself cannot give rise to the observed nearly dissipationless metallic conductivity. Therefore, the coexistence of a pinned CDW and metallic conductivity demands a channel for coherent charge transport. In order to defy all the scattering with the CuO_2 phonons, the free carriers must "ride" the density wave. In the case of a one-dimensional CDW, formation of topological charged solitons (phase kinks) is a possibility.²¹ However, because of the topological nature of the solitons, it requires that both soliton and antisoliton must hop to the neighboring CDW chains to transport charges.

Therefore, the observed coherent charge transport will not take place through the soliton hopping mechanism. In the stripe model,²² each stripe in the CuO_2 plane is considered as a river of charge and conducting.²³ Hence, no charge gap or pinned collective modes are expected. This point has been verified through the transport²⁴ and infrared studies of static charge stripes in $\text{La}_{1.6-x}\text{Nd}_{0.4}\text{Sr}_x\text{CuO}_4$ systems.²⁵ Therefore, our observation bears neither the signature of the idea of strings of charges, either static or dynamic, nor the one-dimensional CDW's in the CuO_2 plane.

The other possibility is a 2D Wigner lattice.²⁶ The observed data may imply that charges (holes in our case) added to the CuO_2 planes condense to form a 2D Wigner lattice. The repulsive Coulomb interaction between the holes at dilute concentration enables the holes to form a 2D square lattice in the CuO_2 plane. In this model, the $\omega = 0$ Goldstone mode of the Wigner lattice has been shifted to $\omega_{GL} \sim 23 \text{ cm}^{-1}$ due to the commensuration pinning of the Wigner lattice to the underlying CuO_2 lattice. Charge-lattice coupling would enhance the lock-in of the Wigner lattice with the underlying CuO_2 lattice¹³ and stabilize the square lattice by lowering the total energy.

Based on the study of the electronic phase diagram at well above room temperature (85°C) where an intrinsic electronic phase instability is observed at exactly $p_c = 1/16$. We can now formally relate our low temperature results to the high temperature special carrier concentration. It seems that this instability survives to low temperature and we suggest that all the doped holes in the CuO_2 plane are condensed to form a (4×4) square Wigner lattice with sides $L = 4a$ ($a = \text{Cu-Cu distance}$). Then, the observed sharp Drude-like free-carrier conductivity in this insulating Wigner lattice ground state comes from the coherent charge transport of the excess holes $\Delta p = p - p_c \sim 0.0005$ per copper which corresponds to $\sim 0.8\%$ of the total carriers in $\delta = 0.024$ sample. In order to achieve such a coherent transport of charges, the free-carriers must reside in a state where the scattering with the phonons of the CuO_2 lattice can be avoided. That is, the free carriers need to "ride" the Wigner lattice. In a

square lattice model, when an excess hole is introduced to the Wigner lattice, it will find an energetically lowest location on the lattice. Because of the on-site Coulomb repulsion at the lattice sites, the minimum energy location would be the center of the square lattice. At this location, the excess hole seats in a local harmonic potential with a zero point energy. This hole now may move because it "sees" a periodic harmonic potential in the directions of the neighboring identical energy minima. This causes the zero point energy of the excess holes to be broadened into a band with the width of which is density dependent. This band is gapped by the Coulomb interaction energy at the minimum energy site. For charge carriers in the Coulomb band, the main energy dissipation channel for electrons is through the scattering with acoustic phonons of the Wigner lattice. At high temperatures, there exists possible promotion of holes from the Wigner lattice site to an interstitial position and vice versa. A similar idea of an interstitial band has been discussed by de Wette for a three-dimensional electron Wigner lattice.²⁷

In this band picture, we anticipate two absorption peaks in addition to the transition across the single particle excitation gap: One due to the transition (ω_1) from the Coulomb band to the single particle excited state and the other involves the transition from the ground state to the Coulomb band (ω_2). However, the ω_2 transition from the ground state to the Coulomb band requires an energy across the gap less the Coulomb energy change in the lattice which is essentially the same as the static Coulomb energy difference between the occupied lattice site and the interstitial lattice site. We suggest that ω_2 is of the order of ~ 0.012 eV (~ 100 cm⁻¹) as seen in the oxygen gas effusion experiments.²⁸ This implies that the Coulomb energy difference between the occupied lattice site and the interstitial lattice site is ~ 0.025 eV. Therefore, we identify the 90 cm⁻¹ peak with ω_1 with a full width $W_c \sim 200$ cm⁻¹ (0.025 eV) and the Coulomb band gap is ~ 300 cm⁻¹. Note that ω_1 and ω_2 are quite close.

The effective mass of the Wigner lattice (m^*) can be estimated by taking the ratio of the oscillator strength of the collective mode (S_{GL}) to that of the single particle excitation ($S_{2\Delta}$) calculated

from the $\sigma_1(\omega)$ and by applying the sum rule

$$S_{GL} + S_{2\Delta} + S_{other} = \pi n e^2 / 2m_e \quad (2)$$

with

$$S_{GL} = \int \sigma_1^{GL}(\omega) d\omega = \pi n_W e^2 / 2m^* \quad (3)$$

and S_{other} is the oscillator strength of all other excitations. Using the experimentally estimated oscillator strengths, we found $m^* \sim 170 m_e$ at 300 K, $\sim 80 m_e$ at 150 K and $\sim 60 m_e$ at 30 K. This implies that the density waves develop the long-range order at $T > 150$ K by drawing its strength from the single particle excitations. We shall see later in the oscillator strength vs. T plot that the crossover occurs at $T_0 \sim 200$ K. However, we believe that m^* is underestimated from the experimental data because the measured reflectivity for frequencies above 400 cm⁻¹ is less than true reflectivity due to the ceramic nature of the sample. In addition, symmetric band is assumed to take into account of the spectral weight above 0.5 eV. Fitting for each peak was made using a symmetric Gaussian function as an approximation without taking into account of asymmetry.

The Debye frequency (ω_D) of the Wigner lattice can be estimated within the harmonic approximation as $\omega_D \approx (e^2 / \epsilon_0 m^* L^3)^{1/2} \sim 42$ cm⁻¹ ($\sim 7.8 \times 10^{12}$ s⁻¹) which gives the Debye temperature (θ_D) of 60 K with $\epsilon_0 \sim 10$, the static dielectric constant of the underlying CuO₂ lattice, and $m^* \sim 60 m_e$. Therefore, we expect the linear T -dependence down to $0.2\theta_D \sim 12$ K²⁹ since the main energy dissipation channel for electrons is the scattering with the acoustic phonons of the Wigner lattice. Through the oscillator strength calculation, we found only $\sim 0.42\%$ of the doped carriers are contributing to the Drude-like conductivity at $T = 300$ K which is consistent with the value estimated from the plasma frequency. This is 50% of the available free carriers at $p = 0.063$ doping. At 300 K, the other 50% may occupy the single particle excited states of the Wigner lattice that might contribute to the incoherent background conductivity. The deviation from the linear T -dependence of the resistivity in under-doped cuprates is due to additional scattering with the lattice defects and domain boundaries whose fluctuation is dynamic as the Wigner

lattice formation is not complete at finite temperatures.

$\sigma_1(\omega)$ of $\delta = 0.032$ sample, which undergoes the superconducting transition at $T_c \sim 26$ K, is displayed in Figure 5a. For $\delta = 0.032$ sample, there are two more structures in $\sigma_1(\omega)$ in addition to those found in $\delta = 0.024$ sample: A sharp peak at $\omega \sim 46$ cm^{-1} and a broader one peaked at $\omega \sim 70$ cm^{-1} . Since we know that the $\delta = 0.032$ sample is right at the fast transition region from a $T_c \sim 15$ K state to a $T_c \sim 30$ K state. It is plausible that the observed $\sigma_1(\omega)$ of $\delta = 0.032$ sample comes from two different contributions; one comes from the $T_c = 16$ K phase (LT_c) seen in $\delta = 0.024$ sample and the other from the $T_c = 30$ K phase (HT_c). Then, the two new features belong to HT_c phase and have their origin in a different Wigner lattice ground state. We identify that the ~ 46 cm^{-1} mode corresponds to the collective mode of this new Wigner lattice, ω_{GH} .

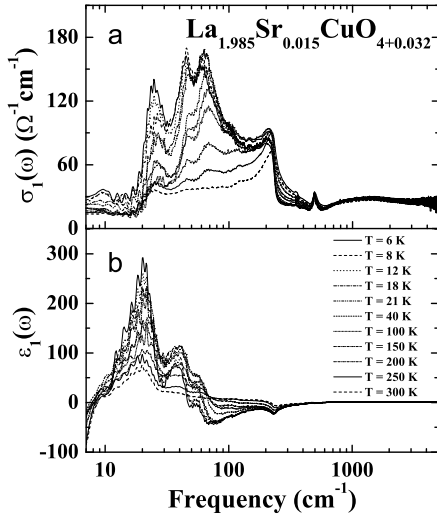


Figure 5. (a) Real part of the conductivity $\sigma_1(\omega)$ and (b) real part of the dielectric function $\epsilon_1(\omega)$ of $\delta = 0.032$ sample.

From the oscillator strengths of the Goldstone

modes, one may determine the ratio of the carrier density in LT_c phase (n_L) and HT_c phase (n_H), n_H/n_L . At 30 K, we find $n_H/n_L \sim 2$, which suggests that the carrier concentration of HT_c phase is twice of that of the LT_c phase when we assume the same m^* . This implies that the HT_c phase contains $c(2 \times 2)$ Wigner lattice, corresponding to $p = 1/8$. That is, the degree of commensuration has been decreased by a factor of two and the corresponding Goldstone mode $\omega_{GH} = 2\omega_{GL}$. We suggest that the physical origin of the so-called $p = 1/8$ anomaly lies in the fact that at $p = 1/8$, the entire holes in the cuprate participate in forming the HT_c phase Wigner lattice. However, we found $n_H/n_L \sim 1.2$ at $T = 300$ K and ~ 2.0 at 150 K suggesting that the HT_c phase grows and builds up the long range order as T is lowered below 300 K. The ~ 70 cm^{-1} peak in the HT_c phase corresponds to the ~ 90 cm^{-1} peak in the LT_c phase. In this new lattice, the Coulomb band gap has increased slightly owing to the decrease in the lattice size of the Wigner lattice.

Based on all the above observations, the normal state properties of cuprates are characterized as following:

(1) Away from half-filling, the new ground state is the 2D Wigner lattice order state and there exists a Coulomb band. Only a small fraction of carriers ($\sim 0.42\%$ at 300 K and $\sim 0.97\%$ at 150 K) in the Coulomb band are participating in the coherent charge transport.

(2) Consequently, there exists two different types of gap; one is the single particle excitation gap at $2\Delta \sim 400$ cm^{-1} and another is the Coulomb band gap on the order of 300 cm^{-1} . We believe this 2Δ is the gap seen in angle resolved photoemission spectroscopy (ARPES), tunneling, and heat capacity measurements, which has been identified as the normal state pseudogap.⁵ In particular, since the best spectral resolution of ARPES is ~ 20 meV (~ 160 cm^{-1}),³⁰ the lower energy excitations than 2Δ have not been resolved in ARPES measurements. However, the observed states within the gap in other experiments have their origin in the density of states of the Coulomb bands.

(3) The Coulomb interaction between free carriers in the Coulomb band is governed by the di-

electric function arising from the presence of the pinned Goldstone mode through

$$\epsilon_1(\omega) = 1 + 4\pi n_W e^2 / m^* (\omega_G^2 - \omega^2) + \epsilon_1(2\Delta) \quad (4)$$

Here, ω_G is the Goldstone mode, n_W is the carrier density in the Wigner lattice and $\epsilon_1(2\Delta)$ is the contribution from the single particle excitation.

Having found that the ground state of cuprates away from half-filling is the Wigner lattice state and the long range Coulomb interactions among the excess carriers in the Coulomb band are massively screened by the presence of the Wigner lattice, any purely attractive interaction will induce the spin singlet pair formation which ultimately gives the superconducting order. The interaction energy between two electrons can be calculated by considering the following Coulomb interaction matrix element between two holes, $\langle H_{12} \rangle$ which takes the form

$$\langle H_{12} \rangle = 4\pi e^2 / q^2 \epsilon_1(q, \omega) \quad (5)$$

Since the holes in the Coulomb band also oscillates in phase with the Wigner lattice at $\omega = \omega_G$ and $1/\epsilon_1(q \rightarrow 0, \omega) \approx 1 - \omega_0^2 / (\omega_G^2 - \omega^2 + \omega_0^2)$ in the long wavelength limit with $\omega_0^2 \equiv 4\pi n_W e^2 / m^*$, one immediately finds the range of ω where $V = \langle H_{12} \rangle$ is attractive as $\omega_G < \omega < \sqrt{\omega_0^2 + \omega_G^2}$. Here we have ignored the contribution from the single particle excitation and the damping of ω_G . Notice that this interaction is not retarded. Therefore, the free carriers in the Coulomb band already form pairs once the long range order of the Wigner lattice develops for temperatures below $T \sim \omega_0 \sim 215$ K. Only when the photon energy greater than ω_0 (or $T > \sim 215$ K), these preformed pairs dissociates via the Coulomb repulsion. In fact, vortex-like excitations in $\text{La}_{2-x}\text{Sr}_x\text{CuO}_4$ systems at T as high as 150 K have been observed in the measurements of the Nernst effect.³¹

How does the superconducting order set in at $T = T_c$? There are evidences supporting that the phase stiffness of the superconducting order parameter $\Psi \sim \Delta e^{i\phi}$ plays a crucial role in high T_c cuprates.³² Even though the pairing of the holes is achieved, the superconducting order will be obtained only after the long-range order in phase

has been established. In conventional BCS superconductors, because of the phase stiffness energy is much greater than the pair binding energy, the transition to the normal state is achieved by breaking the pair at $T \geq T_c$ and the superconducting transition and pairing take place at the same temperature.

In the original BCS theory, the derivation of the Meissner effect from the reduced BCS Hamiltonian is not gauge invariant. From consideration of gauge invariance, Bogoliubov³³ pointed out that there exist collective excited states of quasi-particle pairs, which can be excited only by the longitudinal current associated with the longitudinal component of the vector potential. Therefore, once the superconducting order has been established in ordinary BCS superconductors, the phase collective mode is present due to the broken gauge symmetry and the presence of such collective states is essential for the gauge invariance in the long wavelength limit ($q \rightarrow 0$).

Nambu³⁴ found that the charge density correlation in the ground state is given by $X(q, \omega) \approx n_F q^2 / m_e (\omega^2 - n_F q^2 / N(0))$ where n_F = free electron density and $N(0)$ = density of states. In the presence of the Coulomb interaction between electrons, the dispersion relation for the collective excitations can be determined from the secular equation, $1 - V(q)X(q, \omega) = 0$ with bare Coulomb interaction $V(q) = 4\pi e^2 / q^2$. This secular equation gives $\omega_\phi^2 \sim 4\pi n_F e^2 / m_e$ in $q \rightarrow 0$ limit which is the plasma frequency of the electron gas. This collective mode is known as the Bogoliubov-Anderson mode.³⁵ This mode shifts to the plasma frequency makes the observation of the phase collective mode impossible. However, for the case of the Wigner lattice ground state, we propose that one must consider the screened Coulomb interaction in the Wigner lattice ground state as

$$V(q, \omega) = 4\pi e^2 / q^2 \epsilon_1(q, \omega) \quad (6)$$

instead. This modification leads to the phase collective mode solution $\omega_\phi^2 \approx \omega_G^2 / (1 + \gamma)$ in $q \rightarrow 0$ limit with $\gamma \equiv n_W m_e / n_F m^*$ for the electrons pairs in the Wigner lattice with $\epsilon_1(\omega) \approx 1 + 4\pi n_W e^2 / m^* (\omega_G^2 - \omega^2)$. This implies that the phase collective mode ω_ϕ occurs when the

pairs of electrons in 2D Wigner lattice undergo the Kosterlitz-Thouless transition at $T = T_c$.

The temperature dependence of the oscillator strength of the Goldstone modes and the Coulomb bands of $\delta = 0.024$ and $\delta = 0.032$ samples, plotted in Figure 6 and Figure 7 respectively, are consistent with this picture. Two main remarkable changes are clearly seen; one is a relatively abrupt increase in the oscillator strength at ~ 200 K, common to all the peaks and the other is a sharp jump in the strength of the Goldstone modes, ω_{GL} and ω_{GH} , at their respective superconducting T_c , one at 16 K and the other at 30 K. The increase in the oscillator strength of the collective modes at 200 K, indicates that the long-range order of the Wigner lattice starts to develop as evidenced by the reduction in their dynamic mass. At the same time, the strength increase in the Coulomb band suggests that more carriers occupy the Coulomb band following the development of the long-range order of the Wigner lattice. The corresponding free-carrier oscillator strength changes from $\sim 0.42\%$ at 300 K to $\sim 0.97\%$ at 150 K and to $\sim 1.18\%$ at 30 K in $\delta = 0.024$ sample indicates that all the available free carriers are now occupying the Coulomb band and participating in the charge transport at T below 200 K. However, we do not observe the change in the free carrier plasma frequency because of the increasing static dielectric constant with decreasing T . In $\delta = 0.032$ sample, the free carrier strength is $\sim 0.44\%$ of the total carrier at 300 K and $\sim 0.71\%$ at 30 K. At the same time, as demonstrated above, at the crossover temperature ($T_0 \sim 200$ K) of the long-range order of the Wigner lattice, the free carriers in the Coulomb band start to form pairs. Subtle changes in the $d\rho/dT$ vs. T curves of both $\delta = 0.024$ and $\delta = 0.032$ samples at ~ 200 K has already been pointed out (see Figure 2). The resistivity decreases faster and faster upon cooling below 200 K. Therefore, we have normal state pairs of holes formed at 200 K in our cuprate system. It is interesting to note that 200 K is exactly the temperature when mobile excess oxygen is considered to be frozen in.

We propose that the abrupt increase of the oscillator strength of the Goldstone mode at T_c is

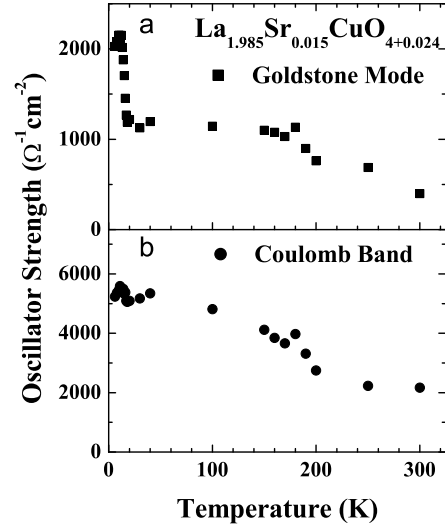


Figure 6. Oscillator strength of (a) the Goldstone mode and (b) the Coulomb band of $\delta = 0.024$ sample versus temperature plot.

resulted from the development of the phase collective mode at $T = T_c$ under $\gamma \ll 1$ condition ($m^* \gg m_e$ and $n_W > n_F$), which gives $\omega_\phi \sim \omega_G$. The abrupt increase of the oscillator strength of ω_{GL} mode at 16 K and ω_{GH} mode at 30 K confirms the development of the phase collective mode of the superconducting order as the phase coherence develops at T_c . Below T_c , the phase of the superconducting order parameter propagates as a collective mode. From the data, $T_c \sim 16$ K is measured with $\hbar\omega_{GL} \approx 23 \text{ cm}^{-1}$ and $T_c \sim 30$ K with $\hbar\omega_{GH} \approx 46 \text{ cm}^{-1}$. Therefore the superconducting T_c can be predicted by measuring the Goldstone mode frequency via $k_B T_c \approx 0.5 \hbar\omega_G$. In fact, the phase collective mode and the Goldstone mode (or the hint of their presence) have been observed in a number of cuprate systems.^{36–47} Specifically, we believe that the mode observed at $\sim 80 \text{ cm}^{-1}$ in the underdoped $\text{Bi}_2\text{Sr}_2\text{CaCu}_2\text{O}_{8+\delta}$ ($\text{Bi}2212$) ($T_c = 67$ K) by Timusk et al.⁴³ is the phase collective mode associated with the pinned Goldstone mode at $\sim 93 \text{ cm}^{-1}$ with $\gamma \sim 2.8$. Also, in their far-

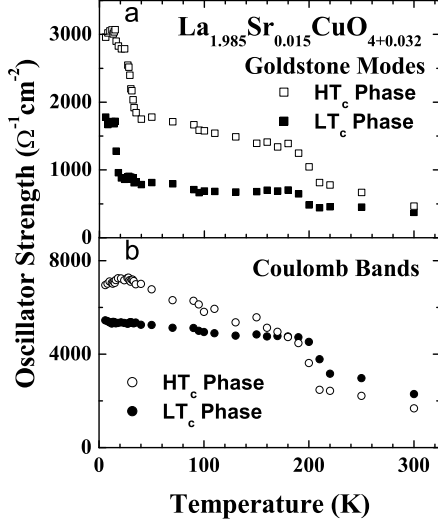


Figure 7. Oscillator strengths of the two Goldstone modes, one for $T_c = 16$ K (LT_c phase) and the other for $T_c = 30$ K (HT_c phase), and the corresponding oscillator strength of the Coulomb bands of $\delta = 0.032$ sample. Each oscillator strength was calculated from the real part of the conductivity by fitting with a symmetric Gaussian function. (See the text for details.)

infrared study of $Tl_2Ba_2CuO_{6+\delta}$, Timusk et al.⁴⁴ reported an observation of a peak at 70 cm^{-1} below $T_c = 88$ K which accompanies a satellite peak at $\sim 120\text{ cm}^{-1}$. This 70 cm^{-1} mode is the phase collective mode with $\gamma \sim 2.0$. The large γ implies the reduction in the dynamic mass of the Wigner lattice compensated by the increase in n_F , free carrier density. Since the oscillator strength of the single particle excitation may be approximated as $S_{2\Delta} \sim \pi n e^2 (1 - n_W m_e / nm^*) / 2m_e$ with $n = n_W + n_F$, the reduction in the dynamic mass of the lattice diminishes the oscillator strength as actually seen in their in-plane conductivities.

In summary, focusing on the special hole concentration $p_c = 1/16$, we have studied the charge dynamics of Sr- and O- co-doped $La_{1.985}Sr_{0.015}CuO_{4+\delta}$ with $\delta = 0.024$ ($p = 0.063$

per Cu) and $\delta = 0.032$ ($p = 0.07$). We observed the Goldstone mode of $p(4 \times 4)$ Wigner lattice corresponding to $p_c = 1/16$ for $p = 0.063$ sample and the Goldstone mode associated with $c(2 \times 2)$ Wigner lattice ($p_c = 1/8$) in addition to the contributions of the $p(4 \times 4)$ lattice for $p = 0.07$ sample. We found that the presence of 2D Wigner lattice and the pinned Goldstone mode is essential for the cuprate physics and superconductivity. We propose that all the high T_c physics are based on the existence of these peculiar 2D electron lattices which are realized by carrier doping into an antiferromagnetic background.

Acknowledgment We would like to thank Zungang Li, Zheng Wu and Young Seok Song for their various technical assistances as well as sample preparations and characterizations during the entire course of this study. We thank John Markus for his genuine interest and technical helps to expedite our experiment. We are also indebted to Bob Hansen at R.G. Hansen and Associates for kindly lending us their liquid helium transfer line during the critical moment of this experiment. PHH is supported by the State of Texas through The Texas Center for Superconductivity at the University of Houston.

REFERENCES

1. F.C. Zhang and T.M. Rice, *Phys. Rev.* **B37**, 3759 (1988).
2. J. Hubbard, *Proc. R. Soc. London, Ser.* **A243**, 336 (1957).
3. P.W. Anderson, *Science* **256**, 1526 (1991); *Phys. Rev. Lett.* **67**, 2092 (1991).
4. S.-C. Zhang, *Science* **275**, 1089 (1997).
5. For a review see T. Timusk and B. Statt, *Rep. Prog. Phys.* **62**, 61 (1999).
6. T.M. Rice, *Physica* **C282-287**, xix-xxiii (1997); B. Batlogg, *Physica* **C282-287**, xxiv-xxx (1997).
7. P. H. Hor et al, to be submitted.
8. Z. G. Li, H. H. Feng, Z. Y. Yang, A. Hamed, S. T. Ting, P. H. Hor, S. Bhavaraju, J. F. DiCarlo, and A. J. Jacobson, *Phys. Rev. Lett.* **77**, 5413 (1996).
9. S. L. Cooper, G. A. Thomas, J. Orenstein, D. H. Rapkine, M. Capizzi, T. Timusk, A. J. Mil-

- lis, L. F. Schneemeyer, and J. V. Waszczak, *Phys. Rev.* **B40**, 11358 (1989); K. Kamarás, S. L. Herr, C. D. Porter, N. Tache, D. B. Tanner, S. Etemad, T. Venkatesan, E. Chase, A. Inam, X. D. Wu, M. S. Hegde, and B. Dutta, *Phys. Rev. Lett.* **64**, 84 (1990).
10. D.B. Tanner and T. Timusk, in *Physical Properties of High Temperature Superconductors*, edited by D.M. Ginsberg (World Scientific, Singapore, 1992), Vol. 3.
 11. M. Reedyk and T. Timusk, *Phys. Rev. Lett.* **69**, 2705 (1992).
 12. D. Munzar, C. Bernhard, and M. Cardona, *Physica* **C312**, 121 (1999); J. Carbotte, E. Schachinger, and D.N. Basov, *Nature* **401**, 354 (1999).
 13. Y. H. Kim, A. J. Heeger, L. Acedo, G. Stucky, and F. Wudl, *Phys. Rev.* **B36**, 7252 (1987); Y.H. Kim, S-W. Cheong, and Z. Fisk, *Phys. Rev. Lett.* **67**, 2227 (1991).
 14. Y.H. Kim, S-W. Cheong, and Z. Fisk, *Physica* **C200**, 201 (1992).
 15. H. H. Feng, Z. G. Li, P. H. Hor, J. F. DiCarlo, S. Bhavaraju, and A. J. Jacobson, *Phys. Rev.* **B51**, 16499 (1995).
 16. Z. G. Li and P. H. Hor in *Stripe and Related Phenomena*, ed. Bianconi and Saini, (Kluwer Academic/Plenum Publishers, New York, 2000), p. 515.
 17. K. Tamasaku, Y. Nakamura, and S. Uchida, *Phys. Rev. Lett.* **69**, 1455 (1992); D.N. Basov, H.A. Mook, B. Dabrowski, and T. Timusk, *Phys. Rev.* **B52**, 13141 (1995); J.H. Kim, H.S. Somal, M.T. Czyzyk, D. van der Marel, A. Wittlin, A.M. Gerrits, V.H.M. Duijn, N.T. Hien, and A.A. Menovsky, *Physica* **C247**, 297 (1995); R. Henn, J. Kircher, and M. Cardona, *Physica* **C269**, 99 (1996); S. Uchida and K. Tamasaku, and S. Tajima, *Phys. Rev.* **B53**, 14558 (1996).
 18. P.H. Hor, H.H. Feng, Z.G. Li, J.F. DiCarlo, S. Bhavaraju, and A.J. Jacobson, *J. Phys. Chem. Solids* **Vol 57**, Nos 6-8, 1061 (1996).
 19. K.H. Kim, Ph.D. Dissertation, University of Cincinnati (1996).
 20. See for a review, G. Grüner, *Rev. Mod. Phys.* **60**, 1129 (1988).
 21. S.A. Brazovskii, *Soviet Phys. JETP* **51**, 342 (1980).
 22. S.A. Kivelson, E. Fradkin, and V.J. Emery, *Nature* **393**, 550 (1998).
 23. J.M. Tranquada, B.J. Sternlieb, J.D. Axe, Y. Nakamura, and S. Uchida, *Nature* **375**, 561 (1995).
 24. T. Noda, H. Eisaki, S. Uchida, *Science* **286**, 265 (1999).
 25. S. Tajima, N.L. Wang, N. Ichikawa, H. Eisaki, S. Uchida, H. Kitano, T. Hanaguri, and A. Maeda, *Europhys. Lett.* **47**, 715 (1999).
 26. E. Wigner, *Phys. Rev.* **46**, 1002 (1934).
 27. F.W. de Wette, *Phys. Rev.* **135**, A287 (1964).
 28. A. Hamed and P. H. Hor, to be submitted.
 29. C. Kittel, in *Introduction to Solid State Physics*, 3rd Ed. (John Wiley and Sons, New York, 1966), p. 220.
 30. Z.-X. Shen and J.R. Schrieffer, *Phys. Rev. Lett.* **78**, 1771 (1997).
 31. Z.A. Xu, N.P. Ong, Y. Wang, T. Takeshita, and S. Uchida, *Nature* **406**, 486 (2000).
 32. V.J. Emery and S.A. Kivelson, *Nature* **374**, 434 (1995).
 33. N.N. Bogoliubov, *Soviet Phys. JETP* **34**, 41 (1958).
 34. Y. Nambu, *Phys. Rev.* **117**, 648 (1960).
 35. P.W. Anderson, *Phys. Rev.* **110**, 827 (1958); *Phys. Rev.* **112**, 1900 (1958).
 36. A.V. Pronin, B.P. Gorshunov, A.A. Volkov, H.S. Somal, D. van der Marel, B.J. Feenstra, Y. Jaccard, and J.-P. Locquet, *JETP Lett.* **68**, 432 (1998).
 37. T. Startseva, T. Timusk, A.V. Puchkov, D.N. Basov, H.A. Mook, M. Okuya, T. Kimura, and K. Kishio, *Phys. Rev.* **B59**, 7184 (1999).
 38. L. D. Rotter, Z. Schlesinger, R. T. Collins, F. Holtzberg, C. Field, U. W. Welp, G. W. Crabtree, J. Z. Liu, Y. Fang, K. G. Vandervoort, and S. Fleshler, *Phys. Rev. Lett.* **67**, 2741 (1991).
 39. T. Pham, M.W. Lee, H.D. Drew, U. Welp, and Y. Fang, *Phys. Rev.* **B44**, 5377 (1991).
 40. D. N. Basov, A. V. Puchkov, R. A. Hughes, T. Strach, J. Preston, T. Timusk, D. A. Bonn, R. Liang, and W. N. Hardy, *Phys. Rev.* **B49**, 12165 (1994).
 41. D.N. Basov, R. Liang, D.A. Bonn, W.N. Hardy, B. Dabrowski, M. Quijada, D.B.

- Tanner, J.P. Rice, D.M. Ginsberd, and T. Timusk, *Phys. Rev. Lett.* **74**, 598 (1995).
42. H.S. Somal, B.J. Finstra, J. Schüzmann, J.H. Kim, Z.H. Barber, V.H.M. Duijn, N.T. Hien, A.A. Menkovski, M. Palumbo, and D. van der Marel, *Phys. Rev. Lett.* **76**, 1525 (1996).
43. T. Timusk, A.V. Puchkov, D.N. Basov, and T. Startseva, *J. Phys. Chem. Solids* **59**, 1953 (1998).
44. T. Timusk, D.N. Basov, C.C. Homes, A.V. Puchkov, and M. Reedyk, *J. Superconductivity* **8**, 437 (1995).
45. N.L. Wang, A.W. McConnell, B. P. Clayman, and G.D. Gu, *Phys. Rev.* **B59**, 576 (1999).
46. C.C. Homes, D. A. Bonn, R. Liang, W. N. Hardy, D. N. Basov, T. Timusk, and B. P. Clayman, *Phys. Rev.* **B60**, 9782 (1999).
47. C.C. Homes, A.W. McConnell, B.P. Clayman, D.A. Bonn, R. Liang, W.N. Hardy, M. Inoue, H. Negishi, P. Fournier, and R. L. Greene, *Phys. Rev. Lett.* **84**, 5391 (2000).